Programmable Aggregation of Artificial Cells with DNA Signals

Hengming Qiu[1+], Feiran Li[1+], Yancheng Du[1+], Ruixin Li[1], Ji Yeon Hyun[2], Sei Young Lee[2*], Jong Hyun Choi[1*]

[1]School of Mechanical Engineering, Purdue University, West Lafayette, Indiana 47907, USA
[2]Department of Biomedical Engineering, Yonsei University, Wonju, Gangwon 26427, Republic of Korea
[+]These authors contributed equally to this work
*Corresponding Author: jchoi@purdue.edu, syl235@yonsei.ac.kr

ABSTRACT
Cell aggregation is a complex behavior, which is closely related to the viability, differentiation, and migration of cells. An effort to create synthetic analogs could lead to considerable advances in cell physiology and biophysics. Rendering and modulating such a dynamic artificial cell system require mechanisms for receiving, transducing, and transmitting intercellular signals, yet effective tools are limited at present. Here we construct synthetic cells from engineered lipids and show their programmable aggregation behaviors using DNA oligonucleotides as a signaling molecule. The artificial cells have transmembrane channels made of DNA origami that are used to recognize and process intercellular signals. We demonstrate that multiple small vesicles aggregate onto a giant vesicle after a transduction of external DNA signals by an intracellular enzyme, and that the small vesicles dissociate when receiving 'release' signals. This work provides new possibilities for building synthetic protocells capable of chemical communication and coordination.

KEYWORDS
Synthetic cells; vesicles; cell aggregation; membrane pore; DNA nanotechnology; DNA origami

INTRODUCTION

Cell aggregation is an important phenomenon in biology, where cells cluster together upon external cues in a certain environment. Studying the intercellular signaling and cell-cell interactions during the process can thus contribute substantially to the understanding of cell differentiation, migration, and viability.[1-3] It also holds great potential in enhancing tissue engineering research as cell interactions are an essential part of tissue building.[4] Cellular signals released in cell interactions generate growth factors[5] and work together with scaffold matrices contributing to tissue construction. Encouraged by the high importance, considerable research efforts were made on this topic, including signaling mechanisms and associated molecules, kinetics and dynamics of cell aggregation, and related disease treatments.[6-7] Due to the complexity of cellular environments, however, mechanisms for aggregation behaviors have not been fully understood and active controls of the processes are yet to be demonstrated. Therefore, a simplified synthetic system capable of cell-to-cell communication and coordination would help achieve a deeper understanding and precise control of cell interactions and behaviors.[8]

Engineered lipid vesicles, resembling some characteristics of biological cells,[9] are widely used in protocell modeling due to the structural similarity and well developed synthesis.[10] Combined with signaling molecules for protocell controls, a mimicry of cellular behaviors such as migration[7] and biosynthesis have been successfully demonstrated.[11-12] Thus, liposomes are an ideal model for mimicking cellular interaction. The protocell models are important for understanding the origin and evolution of cellular life.[13-14] However, demonstrating robust controllable behaviors requires well-understood molecular signals with high programmability and design capacity. Over the past several years, DNA nanotechnology has been explored to construct and control synthetic cells. DNA self-assembly can produce complex architectures with sub-nanometer precision,[15-17] dynamic nanostructures such as switches and motors,[18-19] and computing devices.[20] The key advantage is DNA's excellent programmability and structural predictability. For example, DNA assemblies were used to stabilize vesicle structures and control their shapes.[21-22] DNA base-pairing was implemented for programmable vesicle fusion.[23-24] Recently, DNA origami was used to mimic the shape and function of naturally occurring membrane protein channels.[25-27] They were incorporated into lipid bilayer membranes and served as pores for biomolecular transport in and out of vesicles.[28] The kinetics of transport process through DNA origami pores was measured with dye molecules.[29] The geometry and chemical functionality of this novel class of artificial nanopores can be rationally designed using computer-aided molecular engineering tools that are available for DNA nanotechnology.[30-33] Protein or peptide membrane pores also offer molecularly defined dimensions; however, their geometry may not be modified as easily as for DNA nanostructures, and their chemical functionalization typically is more cumbersome.[34] These features make DNA-based membrane channels highly promising biomolecular devices for applications in single-molecule biosensing and drug delivery, or as components for artificial cells.[35]

In this study, we demonstrate programmable communication and coordination between artificial cells by using transmembrane pores made from DNA origami. The engineered vesicles interact with each other and perform reversible and controllable aggregations in the same manner as biological cells. We have developed new signaling mechanisms for providing biochemical instructions and directing clustering behaviors of the synthetic cells. A set of external biomolecular signals are recognized and transported into the vesicles via transmembrane DNA channels, where they are transduced to another form of signals. The processed signals can then move out of the cells through the origami pores and initiate cell aggregation. In our experiment, DNA oligonucleotides are used as signaling molecules to trigger association and dissociation of vesicles. The aggregation behaviors are monitored with epi-fluorescence microscopy and Förster resonance energy transfer (FRET) measurements. Our system successfully mimics biological cell

behaviors and provides a new model for understanding cellular signal pathways. This work could be valuable for cell biology research with controllable signals for cell growth and differentiation, and inspire new development in bottom-up synthetic biology.

RESULTS AND DISCUSSION

Figure 1 presents the scheme of our experiment. Two types of DNA-decorated vesicles are prepared. Giant unilamellar vesicles (GUVs) are assembled by an inverted emulsion method with diameters ranging from 5 to 25 μm and served as the aggregation core. Small unilamellar vesicles (SUVs) are synthesized with a dehydration-rehydration method with an average diameter of approximately 200 nm (see Materials and Methods section for experimental details).[36-37] The SUVs are designed to dynamically aggregate onto the GUVs, following biochemical signals. The membrane of the giant vesicles contains tubular DNA origami pores that are designed to have a diameter of ~32 nm and a length of ~60 nm (Figures S1 and S2). Each DNA pore is functionalized with cholesterol moieties at the half length to insert the origami in the GUV membrane during the assembly and stabilize it in the hydrophobic lipid environment. These giant vesicles are immobilized on a glass coverslip via biotin-streptavidin conjugation (Figure 1a). The coverslip is sandwiched with a glass slide forming a microfluidic channel and used as the imaging plane for epi-fluorescence microscopy (see Materials and Methods section for details). The glass coverslip is passivated with biotin functionalized bovine serum albumin (BSA), and then streptavidin is introduced. The GUV containing biotinylated phospholipids thus binds to the surface and remains there during the experiments.

The tubular DNA pores are initially closed with planar DNA origami caps by using two sets of staple extensions that are complementary to each other. A set of staples on the pore origami have a 16-nucleotide (16-nt) extension, while the rectangular cap includes staples with a 24-nt extension (shown in pink and green in Figure S1, respectively). The binding between the pore and the cap is confirmed by atomic force microscopy (AFM) imaging (Figure S2) and FRET measurement (Figure S4). The closed pores can be opened using a set of 'cap releaser' strands. Each staple extension on the planar origami cap has an 8-nt single-stranded overhang at the 3' end such that fully complementary cap releasers can replace them via toehold-mediated strand displacement,[38] as illustrated in Figure 1b. A hairpin DNA, shown in purple, is used as a signal for cell-cell interactions. This strand has two domains; one is complementary to the strand on the giant vesicle (shown in blue), and the other can hybridize with the DNA on the small vesicles (red). However, these domains are initially shielded within the hairpin structure, thus it cannot bind to the DNA strands on the vesicles before cleavage by Exo III enzymes. Exo III enzymes are chosen due to their high cleavage rate[39] and are functionalized on polystyrene particles with a diameter of ~200 nm, which are encapsulated in the giant vesicle. With the caps removed, the hairpins can enter the GUV via diffusion, where they can be opened by enzymatic reaction (Figure 1c). The cleaved DNA signal can then diffuse out of the GUV and connect the strands on both giant and small vesicles together, resulting in SUV aggregations on the GUV (Figure 1d). To distinguish small and giant vesicles, rhodamine B fluorophore is incorporated in the SUV membrane and imaged with fluorescence microscopy to clearly show aggregation locations on the GUV. The small vesicles will dissociate from the GUV upon introduction of 'SUV releaser' strands. The releaser strands are fully complementary to the linker strands (transduced hairpin signal) and can remove the linkers via strand displacement, thus resulting in a dissociation of small vesicles from the GUV (Figure 1e).

Figure 2 confirms the embedment of DNA origami pores in the GUV membrane. Here we decorated the origami pores with Cy5 dye for fluorescence imaging (Figure S1). The giant vesicles were immobilized on the bottom surface of the microfluidic channel, and the imaging was performed in the presence of glucose oxidase (oxygen scavenger for preventing photobleaching)

under an inverted microscope using a 63x objective lens. In the fluorescence image, a distinct ring in pseudo red color is observed around the vesicle and matches well with brightfield image (Figure 2a), confirming the incorporation of DNA origami pores. In contrast, no fluorescence was observed from the GUV when cholesterol was not used in DNA origami (Figure 2b). This indicates that tubular origami pores are not embedded in the lipid membrane without cholesterol moieties. We then tested molecular diffusion through open transmembrane DNA channels on the giant vesicle (without caps). Here, green fluorescent protein (GFP) and Cy5-labelled 60-nt DNA were used in the measurement. The fluorescent molecules were supplied to the giant vesicles in tris-acetate-ethylenediaminetetraacetic acid (EDTA) buffer containing 10 mM $MgCl_2$ (termed TAEM buffer). The fluorescence intensity inside the GUVs increased shortly after the inflow, as shown in Figure 2c and 2e. Without origami pores, however, fluorophores cannot enter the vesicles, thus no fluorescence is detected (Figure 2d and 2f).

We verify the effectiveness of the planar origami cap with FRET measurement (Figure S4). Fluorescein dye (FAM) and tetramethylrhodamine (TAMRA) are used as the FRET pair, as the FAM fluorescence will be quenched by TAMRA in close proximity through energy transfer. We modify a set of the cap origami staples such that each staple has a 16-nt extension and a FAM moiety nearby. The TAMRA group is attached on 10-nt strands complementary to the staple extensions. When the TAMRA strands hybridize with the cap origami staple extensions, the FAM fluorescence drops drastically. Then, the tubular pore origami is introduced to bind with the planar cap via 16-bp association. This cap-pore binding event displaces the TAMRA strands and thus recovers the FRET signals. The results confirm the effective binding between the caps and the pores, along with the AFM results (Figure S2).

To characterize the outflux through the membrane channels, we measured the kinetics of GFP and Cy5-DNA released from the giant vesicles (Figure 3). The fluorescent molecules were initially encapsulated inside the GUVs containing the DNA pores closed by the planar origami caps. The fluorescence intensity does not change initially, suggesting that no significant leakage of dye molecules with the origami pores closed. When the cap releasers were supplied to the channel (indicated by the black arrows in Figure 3b and 3d), a drastic decrease of fluorescence intensity inside the vesicle was observed within a few minutes. The fluorescence dropped until it reaches around 40% of the initial intensity. To show the drastic changes, we overlaid the fluorescence images (shown in red) at the beginning and end of the measurements with the brightfield images (Figure 3a, 3c, shown in green). We performed additional multiple kinetic measurements for statistical significance as shown in Figures S5 and S6. It is worth noting that the outfluxes of GFP and Cy5-DNA are similar and that a fraction of fluorescent molecules remains inside the vesicle after a long period of time. The fluorescence decrease was curve-fitted with a single-exponential function; the average time constants calculated were approximately 7 and 15 min for GFP and Cy5, respectively (see SI for details). The fast translocation of the molecules provides a kinetic basis for later experiments involving DNA signal transport in and out of the giant vesicles (*vide infra*). The measured timescales agree well with the previously reported value (~15 min) using 40 kDa dextran with fluorescent moiety by Thomsen *et al.*[29]

Next, we examined the DNA-programmed reversible clustering of vesicles. To test the effectiveness of the SUV linkers and releasers, the origami pores and the Exo-III modified particles were not included in the giant vesicle. The small and giant vesicles have unique strands shown in red and blue, respectively, in Figure 1. We first immobilized a giant vesicle on the imaging surface (state (i), Figure 4a). Then, 36-nt SUV linkers with complementary domains to the strands on the small and large vesicles were supplied along with SUVs to the microfluidic channel (indicated by the red arrow). The final concentrations were about 0.1 nM for the SUVs and 10 nM for the SUV linkers. After 10 min incubation, the TAEM buffer was supplied to wash

away unbound small vesicles and excess linker strands. Distinct fluorescence is observed around the large vesicle boundary (state (ii)), indicating that the small vesicles indeed aggregate on the GUV surface as designed. Note that the fluorescence intensity originates from the small vesicles as the giant vesicle does not include any fluorophores in this measurement. We then supplied the SUV releaser strands to the imaging chamber, indicated by the black arrow. The invading strands first engage with the SUV linkers via 6-nt toehold and bind with them fully, removing the linkers from both the small and large vesicles. As a result, the SUVs dissociate from the GUV and the fluorescence intensity drops, as seen in state (iii). The association and disassociation of the small vesicles on the GUV were repeated by adding the linkers and releasers in series. The fluorescence intensity changed accordingly as shown in Figure 4a. In theory, such a reversible aggregation may be cycled indefinitely. However, the repeatability is limited in actual experiments due to nonspecific bindings and accumulation of waste strands.

We also performed FRET experiments to show collective behaviors of vesicle aggregation (Figure S13; also see SI for experimental details). We observed a drastic fluorescence change upon introduction of the linker strands, confirming the association between the vesicles (Figure S14). Dissociation was also evident with the releaser strands. In the control experiments, we replaced the SUV linkers with strands of random sequence (Figure 4b, Figure S14c) which should not base-pair with the strands on the vesicles. Indeed, vesicle aggregation was not triggered, and no significant changes in the fluorescence intensity were observed as shown in Figure 4b and Figure S14. The results confirm that only designed DNA signals can lead to the aggregation behaviors.

Finally, we demonstrated the recognition and transduction of DNA signals through membrane pores for programmable vesicle aggregation. Here we used the 56-nt hairpin that contains complementary domains (same as SUV linker sequence) for the strands on the vesicles. As discussed in Figure 1, the domains are initially shielded, and thus, the hairpins alone cannot induce vesicle aggregation (Figure S12). The hairpin signal must enter the giant vesicle in order to be transduced by Exo III, exposing the SUV-linker domain via enzymatic digestion. The Exo III-modified, fluorescein-labelled polystyrene particles were encapsulated in the giant vesicle during the assembly. The enzyme-particles are too large to pass through the DNA origami pores, thus they float randomly inside the vesicle, shown as yellow dots in the fluorescence image in Figure 5a (state (ix)). The signal recognition and transduction were demonstrated using this giant vesicle with the DNA pores initially closed by the origami caps (state (i)). We first opened the DNA pores with the cap releasers, as indicated by the orange arrow (state (ii)). The hairpins can then enter the vesicle via membrane channels and interact with Exo III enzymes such that the shielding domain will be cut off and the 36-nt SUV-linker signal will be exposed. When the SUV linkers move out of the GUV, they can bind with the oligonucleotides on the small and large vesicles. As a result, the SUVs aggregate on the GUV, showing the circular fluorescence pattern around the giant vesicle (state (iii)). The clustered, small vesicles were then dissociated (state (iv)), when the SUV releasers were introduced (indicated by black arrows), as in Figure 4.

As discussed above, the translocation of signaling oligonucleotides through the DNA membrane channels is relatively fast with a time constant of about 10 min. Thus, the experiment timespan should be enough for the hairpins and cleaved products to translocate through the pores. While the whole experiment duration in Figure 5 is more than 5 hours, the total light exposure time is less than 10 min. Therefore, the photobleaching effect should be minimal. Additional experiments were performed to demonstrate the robustness of the vesicle aggregation (Figures S10 and S11). We also performed FRET measurements to confirm our observation of individual GUVs (see Figure S13 for FRET details). The ensemble data verify the reversible association and dissociation of small and giant vesicles with drastic fluorescence changes (Figure S15a). In control experiments, we replaced the hairpin with a random sequence. The small vesicles did not

aggregate on the GUV with no significant fluorescence change, as expected (Figure 5b, Figure S15c). Finally, it is worth mentioning that the shape of immobilized vesicles may change slightly over time as seen in Figure 5a as well as Figures S9 and S11. It is also notable that with the release signals the fluorescence becomes very weak, yet it does not drop to 0 (Figure 5a). This may be attributed to some nonspecific binding of small vesicles. Overall, our experiment clearly demonstrates the effectiveness of DNA signals in programming aggregation behaviors of artificial cells.

CONCLUSION

In this work, we have demonstrated chemical communication and cooperative behavior of synthetic cells using DNA signals. The key hairpin signal was effective for the purpose, when and only when it was allowed to enter the cell through membrane channels and interact with enzymes. The DNA origami based transmembrane channels were critical for receiving, transducing, and transmitting biochemical signals. The large DNA pores used in our system allow for the translocation of typical biomolecules such as nucleotides and proteins. Adjusting the origami design may demonstrate size-selective translocation or adaptive caps (e.g., opening and closing in response to environmental changes such as pH).

In our experiment, the vesicles produce and receive biochemical signals, and respond to the signal instructions for collective behaviors. The signaling process involves novel DNA sequence designs. Integrating the processable signals with other cellular behaviors such as migration, division, and reproduction[40] could open the door for constructing more complex multicellular behaviors. (i) First, it may be possible to incorporate the vesicles with biological cells to release signaling molecules (*e.g.,* proteins) which will be beneficial in directing cell growth and differentiations.[41] For example, protocells may release cell-apoptosis signals for anti-proliferation of cancer cells or growth factors to facilitate cell culture. The potential challenges may be finding proper signaling molecules and efficient mechanisms for signal production inside the vesicles. (ii) Another interesting topic could be directed fusion or division of vesicles with DNA signals, thus mimicking essential cell life stages. Such an effort will help build protocells with cell-like life cycles.[42-43] (iii) The synthetic cells may be used as a surrogate model system for neuroscience research. For example, an artificial neuronal network could be constructed to study mechanisms for transferring and receiving neurotransmitters. Such a platform could elucidate propagation pathways of sensation, which has been traditionally difficult to study. Overall, we envision that the growing library of DNA nanotechnology tools and advanced engineered protocell models will together open new opportunities for both fundamental sciences and novel biotechnology applications.

MATERIALS AND METHODS

DNA sequence information

The M13mp18 scaffold was supplied by Bayou Biolabs. All the DNA oligomers were purchased from Integrated DNA Technologies. All DNA strands were used directly from the plates or tubes without further purification.

Name	Sequence
SUV strand	TAA CAA CCA AAC CAT TTT T /3CholTEG/
GUV strand	/amine/ GGA CAG AGT GAC ATC
SUV linker	ATG GTT TGG TTG TTA GAT GTC ACT CTG TCC GAA TCA
Hairpin signal containing SUV linker	ATG GTT TGG TTG TTA GAT GTC ACT CTG TCC GAA TCA ACA TCT AAC AAC CAA ACC AT

SUV releaser	TGA TTC GGA CAG AGT GAC ATC TAA CAA CCA AAC CAT
Cap releaser	TGT CAC TCT GTC CGA ATC AGC ACT
Cy5-DNA	/5Cy5/ GGT GGT GGT GGT TGT GGT GGT GGT GGG TCA CTC rArUG TCC GAA TCA GCA CTT TTT TTT TTT

Table 1. Sequences of DNA linker, releaser, and modified strands. The SUV linker can bind with both SUV and GUV strands, thereby connecting SUVs on a GUV. The hairpin strand includes the sequence of SUV linker which may be exposed after digestion of ACA TCT AAC AAC CAA ACC AT by Exo III. The GAA TCA domain in the SUV linker is used as a toehold for strand displacement by the SUV releaser. Similarly, AGT GCT GA in the cap releaser strand is used as the toehold for strand displacement. Note that Cy5-DNA is a chimeric DNA/RNA oligonucleotide with rArU indicating RNA bases.

Lipid information

Lipid in small vesicles	
16:0 PC or DPPC:	1,2-dipalmitoyl-sn-glycero-3-phosphocholine
16:0 Liss Rhod PE:	1,2-dipalmitoyl-sn-glycero-3-phosphoethanolamine-N-(lissamine rhodamine B sulfonyl) (ammonium salt)
Lipid in giant vesicles	
14:0 PC or DMPC	1,2-dimyristoyl-sn-glycero-3-phosphocholine
18:1 Biotinyl PE	1,2-dioleoyl-sn-glycero-3-phosphoethanolamine-N-(biotinyl) (sodium salt)
DSPE-PEG(2000)-DBCO	1,2-distearoyl-sn-glycero-3-phosphoethanolamine-N-[dibenzocyclooctyl(PEG)-2000]

Table 2. The lipids used in the experiments are listed. All the lipids used are purchased from Avanti Polar Inc.

Conjugation of DNA to lipid molecules

DNA-lipid conjugates are used as components of DNA-decorated GUVs. The method for conjugation is as described in a previous report.[8] The method is a two-step process. The first step is a modification of DNA with azide group. The amine modified DNA strands in Table 1 were synthesized with azide-N-hydroxysuccinimide or azide-NHS in dimethylformamide or DMF, and triethylamine (TEA) was added as catalyst. The mixture was incubated at room temperature in shades for two hours to achieve complete reaction. Then, we added 200 µL ethanol and 10 µL 4 mM NaCl into the solution and froze it at -20 °C for 30 minutes to precipitate DNA. The solution was then centrifuged at 20,000 g for 30 minutes. The precipitate was re-dispersed in 200 µL ethanol and centrifuged for several times to remove excess azide-NHS molecules. After centrifugation, the precipitate was dried in vacuum and re-suspended in 1x phosphate buffered saline (PBS). The concentration of synthesized DNA-azide was determined by the absorption of the sample at 260 nm using a Perkin-Elmer Lambda 950 UV/visible/NIR spectrophotometer.

The second step is a conjugation of azide-DNA with DSPE-PEG(2000)-DBCO. DBCO can react with azide by click chemistry. DNA-azide from the last step was mixed with DSPE-PEG(2000)-DBCO at a molar ratio of 1:5. The mixture was then purified with centrifugation and ready for use.

Polystyrene particles with Exo III

Approximately 5 µL 10 µM Exo III enzyme (New England Biolabs) was mixed with 2% polystyrene particle solution (Thermo Fisher Scientific) diluted in 70 µL 2-(N-morpholino)ethanesulfonic acid (MES) buffer (pH 6.0). Then, 5 µL 100 µM 1-ethyl-3-(3-dimethylaminopropyl)carbodiimide (EDC) was added to the mixture as catalyst. In order to keep the activity of Exo III molecules, the mixture was kept at 4 °C for 3 hours. After the reaction was completed, the mixture was purified with the

centrifugation method to remove the excess enzymes. From the absorption measurement with the extinction coefficient of polystyrene particle (~$2x10^9$ $M^{-1}cm^{-1}$ at 660 nm), we estimate an average of 5 Exo III enzymes attached per polystyrene particle.

Assembly of DNA origami structures

In this study, two sets of DNA origami structures were used (see Figure S1 for the design details). The tubular pore origami was designed as a transmembrane channel, while the rectangular origami was used for capping the pore. The two sets of origami structures were assembled separately from respective one pot synthesis.[30-31, 44] The tubular origami pores were prepared by mixing 10 nM scaffold strands, 4× DNA staples, 14× tubular staples (see Table S1 for details), and 160× cholesterol modified DNA in 1× TAEM buffer (an aqueous solution of 40 mM trisaminomethane, 1 mM ethylenediaminetetraacetic acid (EDTA) disodium salt, 20 mM acetic acid, and 10 mM $MgCl_2$ at pH ~8). Note that cholesterol DNA is used for the insertion into lipid membranes. The mixture was then annealed in a Bio-Rad S1000 thermal cycler from 75 °C to 4 °C at -1 °C per minute.

The planar caps were synthesized by mixing 10 nM scaffold strands with 4× DNA staples (Table S2) in 1× TAEM buffer. The annealing of the mixture went from 75 °C to 4 °C at -1 °C per minute in the thermal cycler. The origami pores and caps were purified 3 times by using the centrifugal filter (100 kDa) from Amicon. Then, the purified pores and caps were mixed at 1:2 molar ratio for assembly of capped origami pores. After that, the mixture was annealed from 55 °C to 4 °C at -1 °C per minute in the thermal cycler.

Synthesis of giant vesicles

DNA-lipid molecules synthesized from the previous step was mixed with DMPC at a molar ratio of 1:1000 in a glass vial.[45-47] The solution was then dried in vacuum for 30 minutes to evaporate all solvent and resuspended with 600 µL liquid paraffin. The new solution was sonicated at 50 °C for 3 hours. Lipids will disperse uniformly in the sonicated solution. Then, 10 µL 10 nM DNA origami pores, 5 µL Exo III-particle, both in 1× TAEM were mixed and additional TAEM buffer added to adjust the volume of the mixture to 20 µL. This mixture was added into the liquid paraffin containing lipids and vortexed for 25 seconds to form aqueous droplets. After vortex, the vesicle solution became blurred. Then, 600 µL of this vesicle solution was poured onto 300 µL TAEM buffer and centrifuged for 15 minutes at 8,000 g. The giant vesicles including DNA strands, origami pores, and Exo III-particles were in the precipitates. Both aqueous phase and oil phase supernatants were discarded, and the precipitate was dissolved in TAEM buffer for future use. From the molar ratio of components, we estimate that there are about 3,000,000 DNA-lipid conjugates integrated on the surface of each giant vesicle. For the giant vesicles without membrane pores, the tubular origami was not included in the synthesis.

Small vesicles with DNA strands

Small vesicles with DNA strands were prepared using a dehydration-rehydration method.[48] Cholesterol modified DNA (*i.e.*, SUV strands in Table S1) and rhodamine B functionalized lipid (*i.e.*, 16:0 Liss Rhod PE) were mixed with DPPC at a molar ratio of 1:1:1000 in a glass vial. The solution was dried in vacuum for 20 minutes to let lipids form a dry thin film on the bottom of the vial. Then, 1 mL TAEM buffer was added to the glass vial and the solution was placed on a pre-heat hot plate at ~90 °C. The solution was stirred with a stirring bar at 500 rpm for 1 hour while the temperature was kept the same all the time. After stirring, small vesicle solution was purified by centrifugation with a 30 kDa molecular weight cut off spin column (from Amicon) at 5,000 g for 5 minutes. This process was repeated 6 times to remove unbound lipid and DNA molecules. From the molar ratio of components, we estimate roughly 50 oligonucleotides per small vesicle.

Flow channel assembly
The experiments were conducted with a multi-channel flow cell assembled with a piece of glass coverslip (Schott) and a quartz slide sealed with medical grade acrylic adhesive sheets. The estimate channel volume is approximately 20 μL. Inlet and outlet ports (LabSmith) were glued to the glass slides using epoxy. In the experiments, Tygon microbore tubing was used to connect sample tubes and the flow channel. The assembled microfluidic channel was placed under an inverted fluorescence microscope for optical imaging.

Surface passivation
The piranha washed glass coverslips were passivated with a one-step method to coat BSA-biotin on the coverslip and prevent nonspecific interactions between the vesicles and the glass surface. Before the experiments, approximately 30 μL 5 μM BSA-biotin in TAEM and tween-20 solution was flown into the channel and incubated for 1 hour. Tween-20 was used to fix defects on the coverslip surface, and BSA-biotin was attached to the surface in order for biotin-streptavidin conjugation that immobilizes giant vesicles on the substrate. After the passivation processes, ~30 μL 1 μM streptavidin in TAEM buffer was added to the fluid channel. Streptavidin can attach the GUVs with biotin moieties on the surface.

Imaging system
A custom-built inverted fluorescence microscope (Zeiss Axio Observer D1) was used for imaging. Three diode lasers at 405, 561, and 658 nm (Laserglow) were used as light source. An oil-immersion 63× objective lens from Zeiss was used, and the collected emission light from the sample was imaged with an Andor iXon3 electron multiplying charge coupled device (EMCCD) camera. We imaged fluorescent giant vesicles for a timespan about one hour. The images were taken at a time interval of 120 sec with ~10 mW excitation power and an exposure time of 3 sec. Thus, though our experiment was more than 60 min, the total light exposure time was about 2 to 3 min depending on the timespan of the experiments. Therefore, photobleaching should not affect our experiment and we did not any significant photobleaching effect in our experiment. Full-scale images of a GUV containing cy5-DNA under bright field and epi-fluorescence were shown in Figure S3. The captured images were analyzed with Fiji and the fluorescence intensity was quantified with the software. The average fluorescence signals over the area of the vesicle were determined by selecting a minimum circular area including the vesicle after the measurement.

ACKNOWLEGEMENT
This work was supported by the U.S. Office of Naval Research (award no. N00014-15-1-2707) and National Science Foundation (award no. 1710344). The DNA origami synthesis and characterization were funded by the U.S. Department of Energy (DOE), Office of Science, Basic Energy Sciences (BES) under award no. DE-SC0020673. S.Y.L. acknowledges the support from the Basic Science Research Program through the National Research Foundation of Korea (NRF) funded by the Ministry of Education (NRF-2016R1D1A1A02937019), Republic of Korea.

SUPPORTING INFORMATION
The Supporting Information is available free of charge on the ACS Publications website at DOI:

Design details of DNA origami, staple sequences, preparation and characterization of DNA origami and vesicle samples, control experiments and additional aggregation experiments

CONFLICT OF INTEREST
The authors declare no competing financial interest.

AUTHOR INFORMATION

Corresponding Authors

Jong Hyun Choi - School of Mechanical Engineering, Purdue University, West Lafayette, Indiana 47907, USA; Orcid: 0000-0002-0507-3052; Email: jchoi@purdue.edu

Sei Young Lee - Department of Biomedical Engineering, Yonsei University, Wonju, Gangwon 26427, Republic of Korea; Orcid: 0000-0002-6077-0221; Email: syl235@yonsei.ac.kr

Authors

Hengming Qiu - School of Mechanical Engineering, Purdue University, West Lafayette, Indiana 47907, USA

Feiran Li - School of Mechanical Engineering, Purdue University, West Lafayette, Indiana 47907, USA

Yancheng Du - School of Mechanical Engineering, Purdue University, West Lafayette, Indiana 47907, USA

Ruixin Li - School of Mechanical Engineering, Purdue University, West Lafayette, Indiana 47907, USA

Ji Yeon Hyun - Department of Biomedical Engineering, Yonsei University, Wonju, Gangwon 26427, Republic of Korea

Author Contributions

H. Qiu performed aggregation experiments, analyzed the data and wrote the manuscript. F. Li provided experiment designs, performed kinetic experiments and analyzed the data. Y. Du performed FRET experiments, analyzed the data and revised the manuscript. R. Li designed the DNA origami and performed simulations. J.Y. Hyun provided technical advice for experimental designs. S. Y. Lee designed the experiments and analyzed the data. J. H. Choi conceived the research, analyzed the data, revised the manuscript and supervised the project. All authors have read and approved the manuscript.

REFERENCES

1. Toyoda, T.; Mae, S.-I.; Tanaka, H.; Kondo, Y.; Funato, M.; Hosokawa, Y.; Sudo, T.; Kawaguchi, Y.; Osafune, K., Cell Aggregation Optimizes the Differentiation of Human ESCs and iPSCs into Pancreatic Bud-like Progenitor Cells. *Stem Cell Research* **2015,** *14*, 185-197.
2. Allion, A.; Baron, J.-P.; Boulange-Petermann, L., Impact of Surface Energy and roughness on cell Distribution and Viability. *Biofouling* **2006,** *22*, 269-278.
3. Kaneko, K.; Yomo, T., Cell Division, Differentiation and Dynamic Clustering. *Physica* **1994,** *75*, 89-102.
4. Saltzman, W. M.; Kyriakides, T. R., *Cell Interactions with Polymers*. Academic Press, 2014.
5. Howard, D.; Buttery, L. D.; Shakesheff, K. M.; Roberts, S. J., Tissue Engineering: Strategies, Stem Cells and Scaffolds. *Journal of Anatomy* **2008,** *213*, 66-72.
6. Bridges, A. B.; Hill, A.; Belch, J. J., Cigarette Smoking Increases White Blood Cell Aggregation in Whole Blood. *Journal of the Royal Society of Medicine* **1993,** *86*, 139-140.
7. Pessac, B.; Defendi, V., Cell Aggregation: Role of Acid Mucopolysaccharides. *Science* **1972,** *175*, 898-900.
8. Pan, J.; Du, Y.; Qiu, H.; Upton, L. R.; Li, F.; Choi, J. H., Mimicking Chemotactic Cell Migration with DNA Programmable Synthetic Vesicles. *Nano Letters* **2019,** *19*, 9138-9144.
9. Xu, C.; Hu, S.; Chen, X., Artificial Cells: from Basic Science to Applications. *Materials Today* **2016,** *19*, 516-532.
10. Chen, I. A.; Walde, P., From self-assembled vesicles to protocells. *Cold Spring Harbor Perspectives in Biology* **2010,** *2*, a002170.
11. Chen, I. A.; Salehi-Ashtiani, K.; Szostak, J. W., RNA catalysis in model protocell vesicles. *Journal of the American Chemical Society* **2005,** *127*, 13213-13219.

12. Noireaux, V.; Libchaber, A., A vesicle bioreactor as a step toward an artificial cell assembly. *Proceedings of the National Academy of Sciences* **2004,** *101*, 17669-17674.
13. Schrum, J. P.; Zhu, T. F.; Szostak, J. W., The origins of cellular life. *Cold Spring Harbor Perspectives in Biology* **2010,** *2*, a002212.
14. Solé, R. V.; Munteanu, A.; Rodriguez-Caso, C.; Macía, J., Synthetic protocell biology: from reproduction to computation. *Philosophical Transactions of the Royal Society B: Biological Sciences* **2007,** *362*, 1727-1739.
15. Jones, M. R.; Seeman, N. C.; Mirkin, C. A., Programmable Materials and the Nature of the DNA Bond. *Science* **2015,** *347*, 1260901.
16. Seeman, N. C., Nanomaterials Based on DNA. *Annual Review of Biochemistry* **2010,** *79*, 65-87.
17. Pinheiro, A. V.; Han, D.; Shih, W. M.; Yan, H., Challenges and Opportunities for Structural DNA Nanotechnology. *Nature Nanotechnology* **2011,** *6*, 763-772.
18. Sen, D.; Gilbert, W., A Sodium-potassium Switch in the Formation of Four-stranded G4-DNA. *Nature* **1990,** *344*, 410-414.
19. Pan, J.; Cha, T.-G.; Li, F.; Chen, H.; Bragg, N. A.; Choi, J. H., Visible/near-infrared Subdiffraction Imaging Reveals the Stochastic Nature of DNA Walkers. *Science Advances* **2017,** *3*, e1601600.
20. Liu, Q.; Wang, L.; Frutos, A. G.; Condon, A. E.; Corn, R. M.; Smith, L. M., DNA Computing on Surfaces. *Nature* **2000,** *403*, 175-179.
21. Kurokawa, C.; Fujiwara, K.; Morita, M.; Kawamata, I.; Kawagishi, Y.; Sakai, A.; Murayama, Y.; Nomura, S.-I. M.; Murata, S.; Takinoue, M.; Yanagisawa, M., DNA Cytoskeleton for Stabilizing Artificial Cells. *Proceedings of the National Academy of Sciences of the United States of America* **2017,** *114*, 7228-7233.
22. Franquelim, H. G.; Khmelinskaia, A.; Sobczak, J.-P.; Dietz, H.; Schwille, P., Membrane Sculpting by Curved DNA Origami Scaffolds. *Nature Communications* **2018,** *9*, 811.
23. Stengel, G.; Zahn, R.; Höök, F., DNA-induced Programmable Fusion of Phospholipid Vesicles. *Journal of the American Chemical Society* **2007,** *129*, 9584-9585.
24. Löffler, P. M. G.; Ries, O.; Rabe, A.; Okholm, A. H.; Thomsen, R. P.; Kjems, J.; Voge, S., A DNA-Programmed Liposome Fusion Cascade. *Angewandte Chemie International Edition* **2017,** *56*, 13228-13231.
25. Burns, J. R.; Seifert, A.; Fertig, N.; Howorka, S., A Biomimetic DNA-based Channel for the Ligand-controlled Transport of Charged Molecular Cargo Across a Biological Membrane. *Nature Nanotechnology* **2016,** *11*, 152-156.
26. Bell, N. A. W.; Engst, C. R.; Ablay, M.; Divtini, G.; Ducati, C.; Liedl, T.; Keyser, U. F., DNA Origami Nanopores. *Nano Letters* **2012,** *12*, 512-517.
27. Burns, J. R.; Göpfrich, K.; Wood, J. W.; Thacker, V. V.; Stulz, E.; Keyser, U. F.; Howorka, S., Lipid-bilayer-spanning DNA Nanopores with a Bifunctional Porphyrin Anchor. *Angewandte Chemie International Edition* **2013,** *52*, 12069-12072.
28. Krishnan, S.; Ziegler, D.; Arnaut, V.; Martin, T. G.; Kapsner, K.; Henneberg, K.; Bausch, A. R.; Dietz, H.; Simmel, F. C., Molecular Transport Through Large-diameter DNA Nanopores. *Nature Communications* **2016,** *7*, 12787.
29. Thomsen, R. P.; Malle, M. G.; Okholm, A. H.; Krishnan, S.; Bohr, S. S.-R.; Sørensen, R. S.; Ries, O.; Vogel, S.; Simmel, F. C.; Hatzakis, N. S.; Kjems, J., A Large Size-selective DNA Nanopore with Sensing Applications. *Nature Communications* **2019,** *10*, 5655.
30. Choi, J.; Chen, H.; Li, F.; Yang, L.; Kim, S. S.; Naik, R. R.; Ye, P. D.; Choi, J. H., Nanomanufacturing of 2D Transition Metal Dichalcogenide Materials Using Self-Assembled DNA Nanotubes. *Small* **2015,** *11*, 5520-5527.

31. Li, F.; Chen, H.; Pan, J.; Cha, T.-G.; Medintz, I. L.; Choi, J. H., A DNAzyme-mediated Logic Gate for Programming Molecular Capture and Release on DNA origami. *Chemical Communications* **2016,** *52*, 8369-8372.
32. Douglas, S. M.; Dietz, H.; Liedl, T.; Högberg, B.; Graf, F.; Shih, W. M., Self-assembly of DNA into Nanoscale Three-dimensional Shapes. *Nature* **2009,** *459*, 414-418.
33. Langecker, M.; Arnaut, V.; Martin, T. G.; List, J.; Renner, S.; Mayer, M.; Dietz, H.; Simmel, F. C., Synthetic Lipid Membrane Channels Formed by Designed DNA Nanostructures. *Science* **2012,** *338*, 932-936.
34. Bayley, H., Designed Membrane Channels and Pores. *Current Opinion in Biotechnology* **1999,** *10*, 94-103.
35. Ketterer, P.; Ananth, A. N.; Trip, D. S. L.; Mishra, A.; Bertosin, E.; Ganji, M.; Torre, J. V. D.; Onck, P.; Dietz, H.; Dekker, C., DNA Origami Scaffold for Studying Intrinsically Disordered Proteins of the Nuclear Pore Complex. *Nature Communications* **2018,** *9*, 902.
36. Walde, P.; Cosentino, K.; Engel, H.; Stano, P., Giant Vesicles: Preparations and Applications. *ChemBioChem* **2010,** *11*, 848-865.
37. Morita, M.; Katoh, K.; Noda, N., Direct Observation of Bacterial Growth in Giant Unilamellar Vesicles: A Novel Tool for Bacterial Cultures. *ChemistryOpen* **2018,** *7*, 845-849.
38. Srinivas, N.; Ouldridge, T. E.; Šulc, P.; Schaeffer, J. M.; Yurke, B.; Louis, A. A.; Doye, J. P. K.; Winfree, E., On the Biophysics and Kinetics of Toehold-mediated DNA Strand Displacement. *Nucleic Acids Research* **2013,** *41*, 10641-10658.
39. Henikoff, S., Unidirectional digestion with exonuclease III creates targeted breakpoints for DNA sequencing. *Gene* **1984,** *28*, 351-359.
40. Dzieciol, A. J.; Mann, S., Designs for life: protocell models in the laboratory. *Chemical Society Reviews* **2012,** *41* (1), 79-85.
41. Lentini, R.; Santero, S. P.; Chizzolini, F.; Cecchi, D.; Fontana, J.; Marchioretto, M.; Del Bianco, C.; Terrell, J. L.; Spencer, A. C.; Martini, L., Integrating artificial with natural cells to translate chemical messages that direct E. coli behaviour. *Nature communications* **2014,** *5*, 1-6.
42. Kurihara, K.; Okura, Y.; Matsuo, M.; Toyota, T.; Suzuki, K.; Sugawara, T., A recursive vesicle-based model protocell with a primitive model cell cycle. *Nature communications* **2015,** *6*, 1-7.
43. Mansy, S. S.; Schrum, J. P.; Krishnamurthy, M.; Tobé, S.; Treco, D. A.; Szostak, J. W., Template-directed synthesis of a genetic polymer in a model protocell. *Nature* **2008,** *454* (7200), 122-125.
44. Chen, H.; Wang, T.-W.; Riccitelli, M. M.; Cui, Y.; Irudayaraj, J.; Choi, J. H., Understanding the Mechanical Properties of DNA Origami Tiles and Controlling the Kinetics of Their Folding and Unfolding Reconfiguration. *Journal of the American Chemical Society* **2014,** *136*, 6995-7005.
45. Elani, Y.; Trantidou, T.; Wylie, D.; Dekker, L.; Polizzi, K.; Law, R. V.; Ces, O., Constructing Vesicle-based Artificial Cells with Embedded Living Cells as Organelle-like Modules. *Scientific Reports* **2018,** *8*, 4564.
46. Akbarzadeh, A.; Rezaei-Sadabady, R.; Davaran, S.; Joo, S. W.; Zarghami, N.; Hanifehpour, Y.; Samiei, M.; Kouhi, M.; Nejati-Koshki, K., Liposome: Classification, Preparation, and Applications. *Nanoscale Research Letters* **2013,** *8*, 102.
47. Chiba, M.; Miyazaki, M.; Ishiwata, S., Quantitative Analysis of the Lamellarity of Giant Liposomes Prepared by the Inverted Emulsion Method. *Biophysical Journal* **2014,** *107*, 346-354.
48. Kirby, C.; Gregoriadis, G., Dehydration-Rehydration Vesicles: A Simple Method for High Yield Drug Entrapment in Liposomes. *Bio/Technology* **1984,** *2*, 979-984.

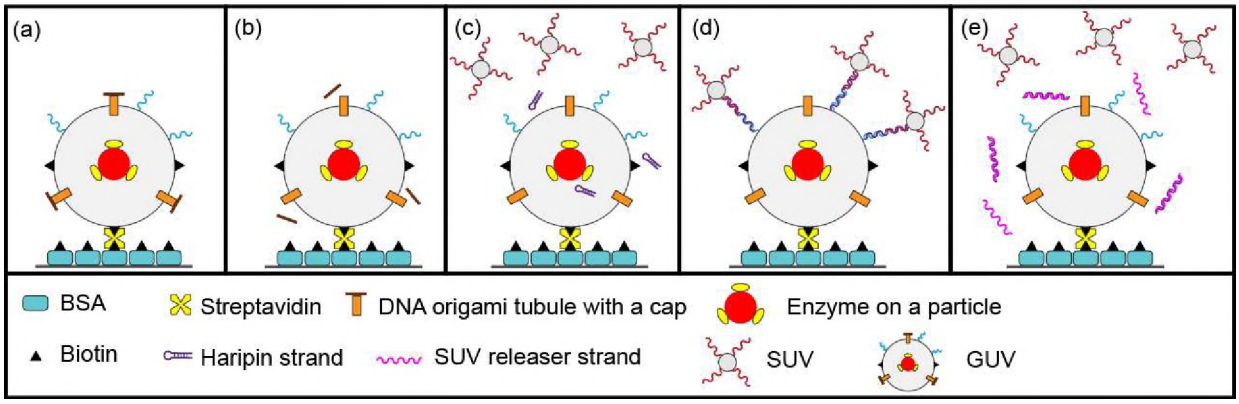

Figure 1. Scheme for reversible cell aggregation programmed by DNA signals. (a) A giant vesicle is immobilized on a BSA modified glass surface by biotin-streptavidin conjugation. The GUV has DNA strands (shown in blue) as binding spots for the SUVs decorated with another set of DNA strands (shown in red). DNA origami pores (oranges) are embedded in the GUV membrane. Exo III enzymes on the polystyrene particle (yellow-red) are encapsulated inside the giant vesicle. (b) The pores are initially closed with flat origami caps which can be removed by 'cap-releaser' strands via toehold-mediated strand displacement. (c) An external DNA hairpin signal can enter the vesicle through the membrane channels where it is transduced into another form of signal via enzymatic reaction by Exo III. The enzyme digests a part of the hairpin from the 3' end, thereby exposing the complementary domains for the strands on the vesicles (blue on the GUV and red on the SUVs). (d) The processed signaling oligonucleotides will pass through the origami pores and trigger aggregation of multiple small vesicles on the GUV. (e) Another DNA signal, 'SUV releaser' strands shown in pink, will dissociate the SUVs bound on the giant vesicle, by removing the linker strands. This association and dissociation behavior can be programmed with DNA signals.

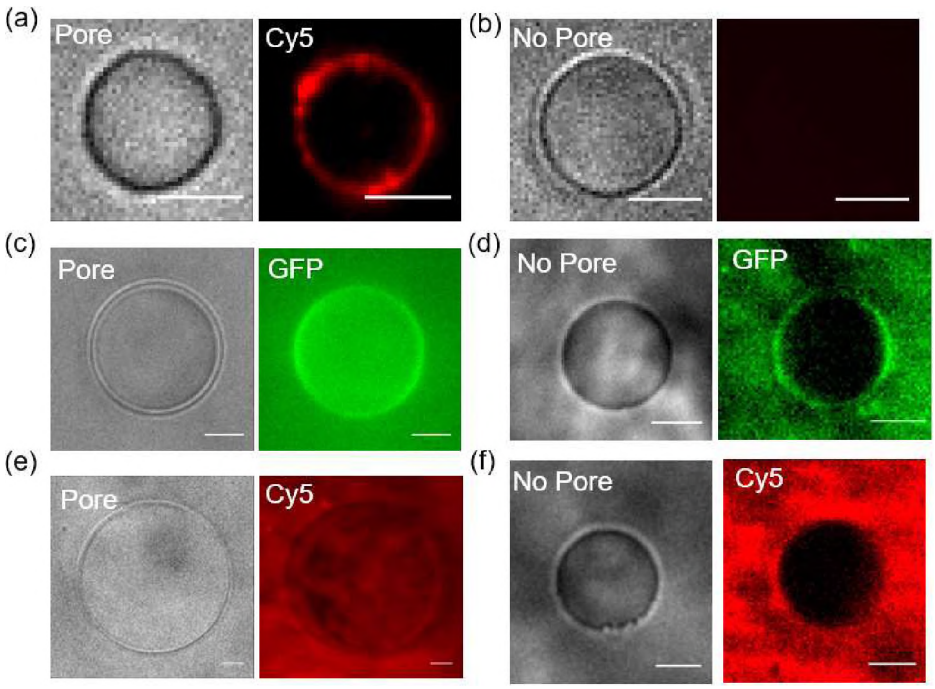

Figure 2. Brightfield (left) and fluorescence (right) images of giant vesicles. In fluorescence images, GFP is shown in green color and Cy5 is represented in red. (a) Cholesterol modified DNA pores are embedded in the vesicle membrane. The Cy5 functionalized origami shows a distinct, ring-shaped fluorescence pattern around the vesicle boundary. (b) DNA origami without cholesterol moieties cannot insert in the membrane, thus no fluorescence is observed. (c) GFP can penetrate into the vesicle via transmembrane channels made of tubular DNA origami. (d) Without DNA pores, GFP cannot diffuse into the vesicle. (e) Cy5-DNA can enter the vesicle with DNA pores. (f) The fluorophore labelled DNA cannot move into the GUV in the absence of origami pores. Note that the origami pores in (c) and (e) are not functionalized with Cy5 dyes. Scale bars are 5 μm.

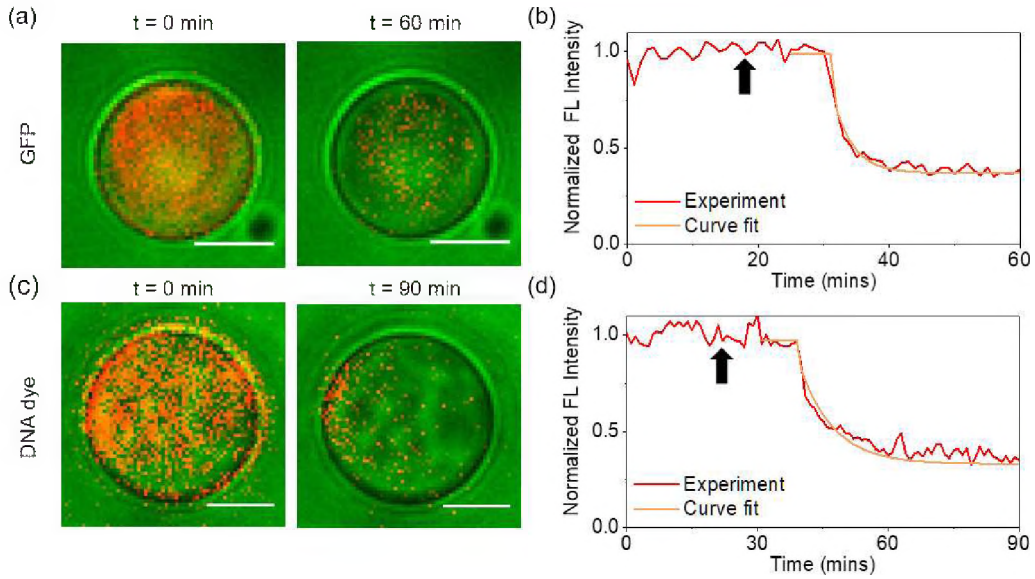

Figure 3. Kinetic measurement of molecular outflux through origami pores from giant vesicles immobilized on the glass coverslip surface. (a) Fluorescence images of GFP molecules (shown in red color) overlaid with brightfield images of a vesicle at time t = 0 and 60 min. The molecules, initially encapsulated in the GUV, diffuse out of the vesicle after the pores are opened. (b) The fluorescence intensity inside the vesicle decreases, shortly after the cap-releaser strands were introduced into the microfluidic imaging chamber (indicated by the black arrow). (c) Fluorescence images of Cy5-DNA inside a giant vesicle overlaid with brightfield images at time t = 0 and 90 min. (d) The fluorescence diminishes after adding the cap releasers (black arrow). Scale bars are 5 μm.

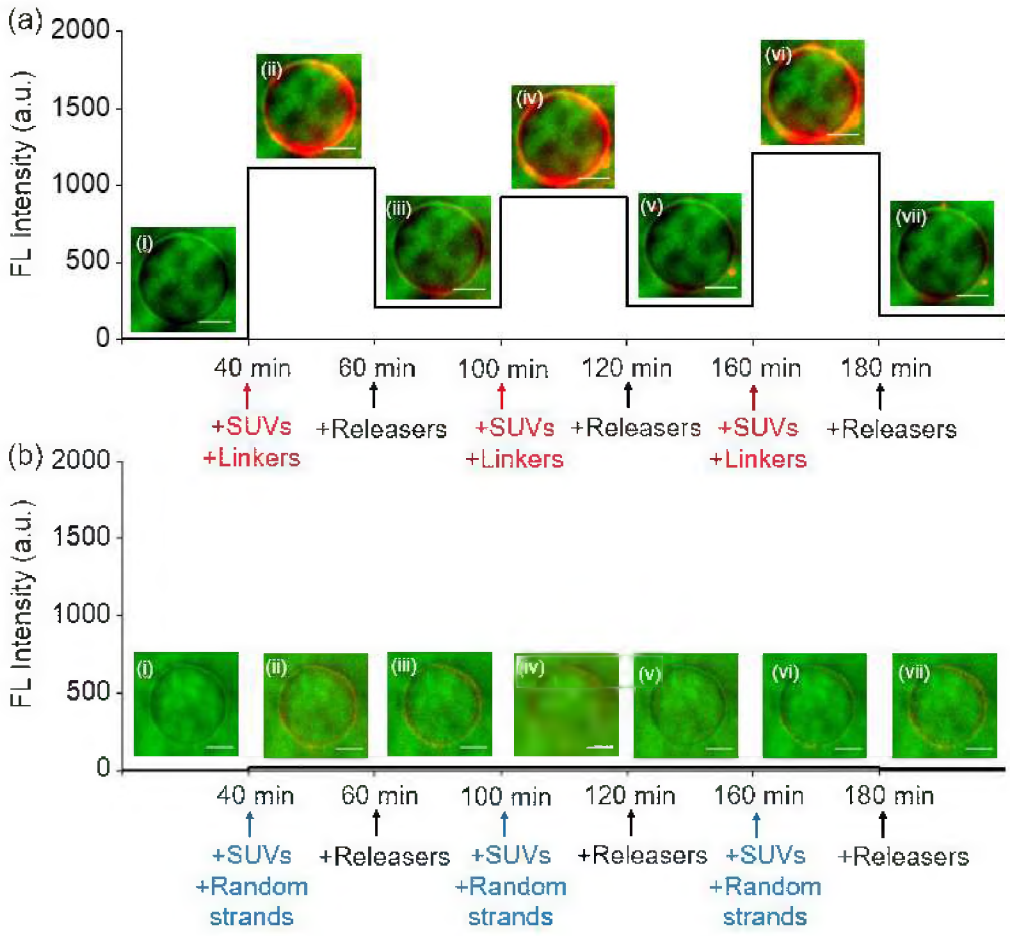

Figure 4. Reversible vesicle aggregation with DNA signals. (a) Fluorescence intensity of the small vesicles around the GUV on each experimental step. Corresponding images of fluorescence overlaid on brightfield images are also presented. The SUVs have oligonucleotides (red strands in Figure 1) and rhodamine B dyes for imaging. The giant vesicle contains DNA strands on its surface (blue strands in Figure 1), but does not include DNA origami pores nor polystyrene particles. (i) A giant vesicle is immobilized on the microfluidic imaging chamber via biotin-streptavidin conjugation. (ii) Small vesicles and 36-nt SUV-linker DNA are introduced (indicated by the red arrow) which will trigger SUV clustering on the giant vesicle via base-pairing of the linkers with the strands on both giant and small vesicles. As a result, the fluorescence intensity increases drastically. (iii) A set of SUV releaser strands are supplied, represented by the black arrow. The signaling oligonucleotides will first bind with the 6-nt toehold and hybridize fully with the SUV-linkers, thus removing the linkers from the vesicles. The small vesicles will thus dissociate from the GUV, and fluorescence intensity drops drastically. (iv)-(vii). The reversible vesicle aggregation can be repeated with DNA signals (SUV linkers and releasers). (b) Control experiment, using a random DNA sequence instead of the SUV linkers (represented by the blue arrows). As anticipated, the small vesicles are not bound on the GUV, thus no significant change in the fluorescence is observed. Scale bars are 5 μm in all images.

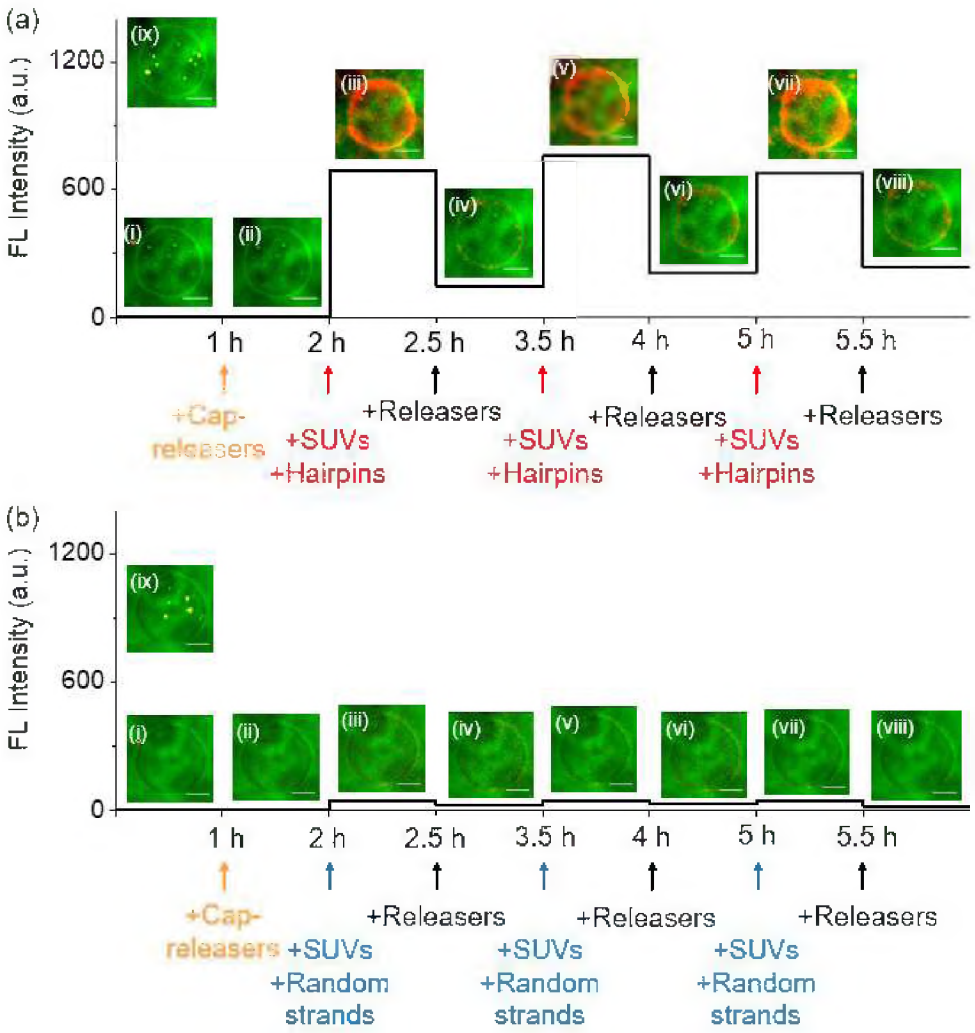

Figure 5. (a) Dynamic aggregation behavior of artificial cells programmed by DNA signals. To receive and transmit signals, tubular origami pores are included in the giant vesicle which also encapsulates Exo-III modified polystyrene particles. (i) A giant vesicle is immobilized on the imaging chamber. (ii) A set of cap releaser strands are supplied to remove the planar origami caps (orange arrow). (iii) The hairpin strands and small vesicles are introduced to the channel, as indicated by the red arrow. The hairpins penetrate into the vesicle through the transmembrane origami channels and are partly digested by Exo III, exposing the SUV linker domain. The transduced oligonucleotides diffuse out through the pores and bind with the strands on the small and giant vesicles. As a result, the small vesicles cluster around the GUV surface, which is evident with a circular fluorescence image overlaid on the brightfield image of the giant vesicle. (iv) When the SUV releasers are introduced (represented by the black arrow), they remove the SUV linkers via toehold-mediated strand displacement. The small vesicles then dissociate from the GUV, and the fluorescence intensity drops drastically. (v)-(viii) The DNA programmable clustering behavior can be repeated multiple times. (b) Control experiment using a random sequence instead of the hairpin. (i)-(ii) The DNA pores are opened by removing the caps (indicated by the orange arrow). (iii) The oligonucleotides of random sequence may enter the giant vesicle (blue arrow), but they cannot trigger the aggregation of small vesicles on the GUV. Thus, no significant changes in the fluorescence are observed (iii). (iv) The addition of SUV releasers will not result in any changes in the behavior of the vesicles. Scale bars are 5 μm in all images. (ix) The polystyrene particles

functionalized with Exo III enzymes are shown as yellow dots. The 200-nm-diameter particles randomly float inside the GUV.

Table of Content